Tetrameric Aryl Palladium Bromide Intermediates Leading to Facile Transmetalation in Suzuki–Miyaura Cross-Couplings with Pd@MIL-101-NH_2(Cr)

Alejandro Valiente,[a] Cheuk-Wai Tai,[b] Mårten Ahlquist,[c] and Belén Martín-Matute*,[a]

[a] Department of Organic Chemistry, Stockholm University, The Arrhenius Laboratory 16C, SE-106 91, Stockholm (Sweden)

[b] Department of Materials and Environmental Chemistry, Stockholm University, The Arrhenius Laboratory 16C, SE-106 91, Stockholm (Sweden)

[c] Department of Theoretical Chemistry and Biology, School of Engineering Sciences in Chemistry,Biotechnology and Health KTH Royal Institute of Technology SE-10691 Stockholm (Sweden)

KEYWORDS: Ligandless; Palladium; Catalytic Intermediates; Mass spectrometry; Palladium trimer; Metal-Organic Framework

ABSTRACT: The composition and structure of catalytic intermediates in the context of the Suzuki–Miyaura cross-coupling reaction catalyzed by Pd@MIL-101-NH_2(Cr) has been investigated. Trimeric and tetrameric palladium species with formula $[Br–Pd–Ar]_nBr^-$ (n = 3–4) have been identified by electrospray ionization mass spectrometry (ESI-MS) and density-functional theory (DFT) calculations, and their role in the transmetalation step has been studied. The weak nature of the bonds between Pd and the bridging halides in these species enables a very easy transmetalation step, with an estimated activation free energy of only 10 kcal/mol. Further experimental support for Pd speciation was obtained using scanning transmission electron microscopy (STEM), inductively coupled plasma-optical emission spectroscopy (ICP-OES), and fluorine-19 nuclear magnetic resonance spectroscopy (^{19}F NMR).

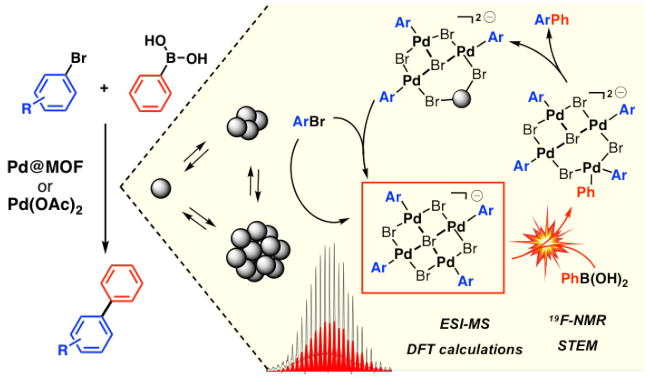

The Suzuki–Miyaura cross-coupling reaction is one of the most efficient methods for the construction of C–C bonds, and it is widely used in industry for the synthesis of building blocks and pharmaceuticals.[1–4] A wide range of palladium catalysts may be used, including palladium nanoparticles (NP) and palladium complexes with or without strong donor ligands.

Catalysts with P-, N-, or NHC-based ligands have been very important for studying the mechanism of Suzuki-Miyaura cross-coupling reactions.[5–14] For example, complexes with ligands bearing NMR-active nuclei (i.e., ^{19}F) have been used to monitor the reactions by NMR spectroscopy.[15] Ligandless systems, i.e., those lacking strong donor ligands, have proved to be highly active catalysts when used at very low catalyst loadings (e.g., parts per million or billion), resulting in turnover numbers (TON) of up to 10^7.[16–25] Often, these palladium species are stabilized by a support (e.g., carbon, polymers, dendrimers, metal-organic frameworks (MOFs),[26–28] quaternary ammonium salts (e.g., NBu_4X, Jeffery system),[29,30] or other additives (i.e., *N,N*-dimethylglycine).[31]

Identifying the composition and morphology of the catalytically active species in ligandless systems, which are generated from Pd salts or from Pd NPs, is a very challenging task. To a large extent, this is due to their low concentration and their dynamic character.[17,32–40] Numerous studies indicate that a "cocktail" of Pd(0) species is involved, and when Pd NPs are used, these species are produced by Pd leaching from the NPs (Figure 1). Despite intense research in this field, very little is known about the structure of the specific intermediates that may be involved in the catalytic cycle, more specifically, in the turnover-limiting step, which for aryl bromides and iodides is usually the transmetalation step.[41] It is has been proposed that the oxidative addition step in the catalytic cycle may involve atomic Pd species in solution (Figure 1).[42,43] Palladium dimers have also been identified and isolated from the reaction mixtures, but these kinetically stable species were considered to be off-cycle

intermediates that enter the catalytic cycle upon cleavage into monomers.[44,45]

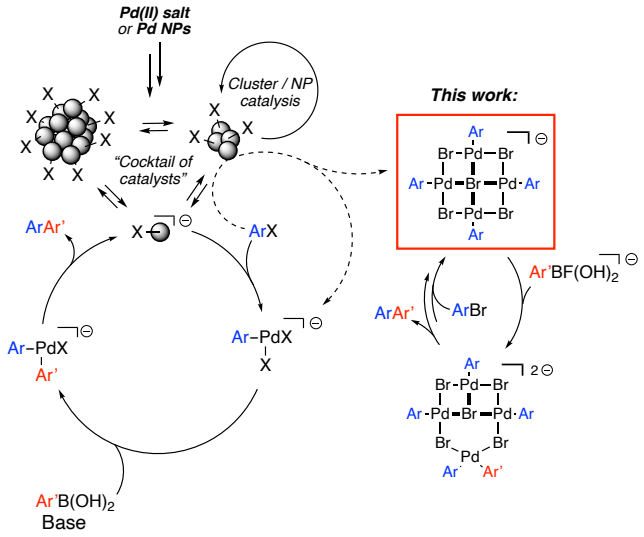

Figure 1. Generally proposed catalytic cycle for the ligand-free Suzuki-Miyaura reaction and intermediacy of oxidative-addition palladium tetramers (this work). Some charges and/or counterions were omitted for clarity.

MOFs have been used as supports for various Pd species, most often NPs, and used as very efficient catalysts in different cross-coupling reactions.[26,46–49] In some instances, spectacular reactivity under very mild conditions has been achieved. This is the case for the Suzuki–Miyaura cross-coupling reaction, where Pd@MOFs such as MOF-253,[50] MOF-5,[51] IRMOF-3,[52] MIL-53-NH_2,[53] and MIL-101[54] have been extensively investigated as catalysts. In particular, we reported the use of Pd@MIL-101-NH_2(Cr) as a catalyst for the coupling of highly functionalized arylboronic acids and aryl halides.[55] The catalyst consisted of evently distributed Pd NPs, with an average size of 2.6 nm.[56] Loadings of palladium as low as 0.01 mol% could be used, under very mild conditions (20 °C) with H_2O/EtOH mixtures as the solvent, resulting in TONs of up to 10000. In contrast, similar palladium nanoparticles immobilized on other supports require very harsh reaction conditions.[17,57–61] With the aim of understanding the distinctive reactivity in all these system, we have now investigated the structure of the Pd species formed in the Suzuki–Miyaura cross-coupling reactions mediated by Pd@MIL-101-NH_2(Cr) by means of electrospray ionization mass spectrometry, ESI(–)-MS, density functional theory (DFT) calculations, and ^{19}F NMR spectroscopy. In this report, we have identified trimeric and tetrameric palladium oxidative addition species as key intermediates in Suzuki-Miyaura cross-couplings catalyzed by Pd@MOF. Importantly, it was found that these intermediates undergo a very facile transmetallation. These species, which have never been proposed before, have also been identified when using other ligandless systems, such as $Pd(OAc)_2$ in absence of strong donor ligands.

We began our study by investigating the coupling reactions of 1-bromo-4-(trifluoromethyl)benzene (**1a**) or 1-iodo-4-(trifluoromethyl)benzene (**1a'**) with phenylboronic acid (**2a**). We compared the catalytic performance of Pd@MIL-101-NH_2(Cr) (2.4 nm average NP size, 7.25 wt% Pd content in the MOF, 3 mol% Pd loading in the catalytic reaction, Figure 2a and Figure S1) with that of the filtrates obtained from these same reactions. The reaction profiles (Figure 2a) show that starting from **1a**, a yield of 94% of **3a** was obtained after only 60 min with the MOF catalyst, which agrees with our previous results.[62] Interestingly, the yield was much lower when the iodide substrate **1a'** was used (35% yield of **3a** after 60 min). The catalytic activity of the filtrates from both reactions was analyzed after 60 min (Figure 2b). After filtration, the filtrate was added to a new load of reactants without additional Pd@MIL-101-NH_2(Cr) (i.e., **1a** or **1a'**, **2a**, and KF) and the mixture was left to react for a further 60 min. For aryl bromide **1a** (filtrate A), an accumulated yield of 90% was obtained, which is similar to the yield obtained by using only Pd@MIL-101-NH_2(Cr) (i.e., 94%, Figure 2a). Filtrate A, obtained from a parallel experiment, was analyzed by inductively coupled plasma optical emission spectroscopy (ICP-OES). This revealed the concentration of palladium to be very low, only 0.1 ppm. Therefore, with this low catalyst loading, a TON of ca 5×10^4 can be estimated. The presence of Pd in filtrate A was also confirmed by scanning transmission electron microscopy (STEM), which showed the presence of crystalline Pd NPs of 4.8 nm average size together with Pd clusters (<1 nm); MOF crystals where not observed (Figure 2c and Figure S2). In contrast, the accumulated yield of **3a** when using aryl iodide **1a'** (18%) indicated that filtrate B was inactive, as the second load of reactants were barely consumed. This result is in contrast with the usual reactivity of aryl iodides *vs* aryl bromides in cross-coupling reactions; the lower bond-dissociation energy (BDE) of C–I *vs.* C–Br bonds is a major factor controlling their oxidative addition to Pd(0) (BDE C–I = 67.2, C–Br = 82.6 kcal/mol).[63] To further assess the nature of the species in filtrate A, we turned into electrospray ionization mass spectrometry (ESI-MS).[40,64–71] Filtrate A obtained after 30 min of t_1 was analyzed by ESI-MS in positive-ion mode, and palladium species were not found (Figure S3). However, a series of substrate-bound palladium adducts were observed in negative-ion mode, specifically in the *m/z* region between 400 and 1450 (Figure 2d). Adducts **4a**–**7a** were identified as oxidative-addition clusters (Pd = 1–4), with anionic tetramer **4a** as the base peak of the spectrum (Figure 2d). The structure of oxidative-addition tetramer **4a** was calculated using density functional theory (DFT) at the B3LYP-D3 level (Figure 2d). Related tetramers, lacking the central bromide, have been computationally proposed,[40] but not observed experimentally.

These calculations indicated that each palladium(II) center in **4a** retains a geometry close to square planar, and that the central bromide is slightly outside of the plane of the four palladium atoms (27°) (Figure 2b). The Gibbs free energy was also calculated to assess the stability of the species, and we found that there is a significant driving force for each step, from monomer to tetramer, at standard state (Figure 3a). Since all intermediates (**4a**–**7a**) are negatively charged, and the reactions are run in aqueous media, $[ArPdBr_2(OH_2)]^-$ (**7a**) and three neutral $[ArPdBr(OH_2)_2]$ species were chosen

as the references. As Pd–OH_2 bonds will be broken in every step and replaced by Pd–Br bridges, which are essentially half bonds, it appears that the driving force for the formation of the higher oligomers (**4a**, **5a**) cannot be the bonding enthalpy. We therefore split the Gibbs free-energy change into the entropic contribution (–TΔS) and the enthalpic contribution (ΔH). We found that for every step there is an unfavorable enthalpic change, except from trimer **5a** to tetramer **4a**, which is minimally exothermic. On the other hand, the entropic contribution favors every step significantly due to the

a)

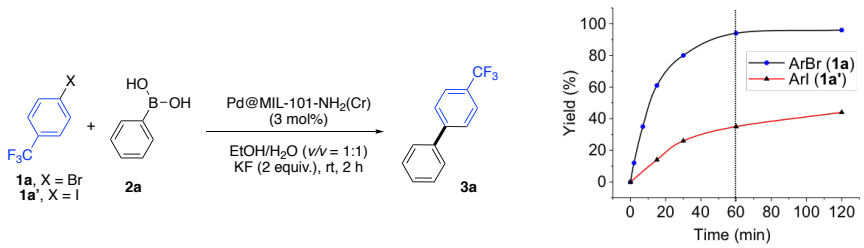

b)

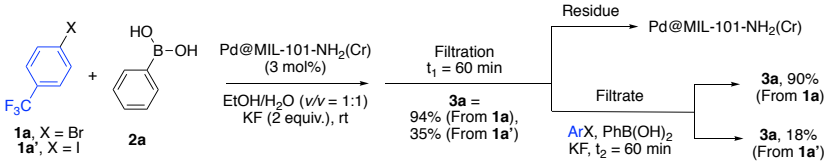

c)

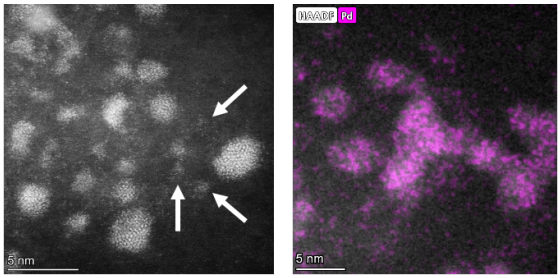

d)

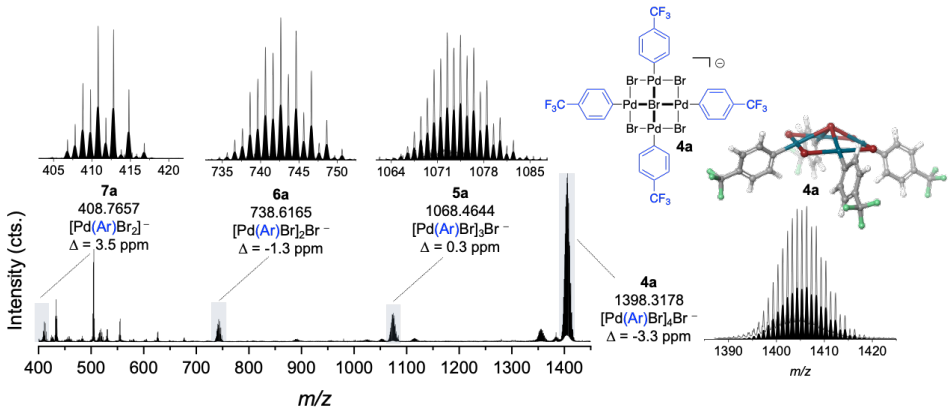

Figure 2. (a) Model Suzuki–Miyaura reaction used in this work (left), and reaction profiles for aryl bromide 1a and aryl iodide 1a' (right); (b) Filtration experiments with aryl bromide 1a and aryl iodide 1a'. Yields were determined by ^{1}H NMR spectroscopy using 1,3,5-trimethoxybenzene as an internal standard; yields after filtration are expressed as accumulated yield (based on the total amount of ArX added); (c) HAADF-STEM image of Pd NPs and clusters in filtrate A (left) and EDX elemental mapping of Pd overlaid of HAADF image (right). Some Pd clusters are indicated with white arrows; (d) Identified adducts in Filtrate A (reaction time = 30 min), indicating measured mass (monoisotopic), formula, and error. Inset shows obtained (grey) and simulated (black) isotopic patterns for each adduct. On the right, 3D structure of 4a from DFT calculations.

release of bound water molecules. The stability of the complexes therefore arises from entropy (released molecules) rather than from enthalpy (released heat). This may have a significant impact on the reactivity, as described below. The calculations showed that the most stable oxidative-addition adduct was tetramer **4a**, and this same adduct was also the one found with the highest relative abundance by ESI-MS.

Analysis by ESI(–)-MS of filtrate B (t = 15 min) from the reaction of iodide **1a'** also indicated the formation of tetrameric (**4a'**) and trimeric (**5a'**) iodide adducts, but monomer **7a'** was found to be the major species (Figure 4a). Analysis of filtrate B after 120 min revealed that tetramer **4a'** and trimer **5a'** had been consumed, and a series of palladium iodide salts with formulas $[Pd_2I_4]_n^-$ (n = 1 or 2) and $[Pd_2I_n]^-$ (n = 3 or 5) were detected (Figure S4). These palladium iodide salts have been previously detected and isolated in other studies, and due to their high stability they were considered off-cycle species.[44,72,73] Their formation may explain the slower kinetics in the reaction of **1b**, as the concentration of active palladium species leading to product is diminished (Figure 2b). This is also in agreement with the findings by Ananikov and coworkers, who determined that in dynamic systems there are factors other than ease of oxidative addition (iodides > bromides) that can affect the efficiency of a process, e.g., the stabilization of Pd(II) and Pd(0) intermediates by halides.[74] Although aryl iodides undergo faster oxidative addition than aryl bromides, iodide anions exert a greater stabilization on Pd(II) than bromide anions, thereby "trapping" these palladium species as kinetically stable salts.

Figure 4b shows the kinetic profile of the reaction (i.e., yield of **3a** over time) catalyzed by Pd@MIL-101-NH_2(Cr) and by $Pd(OAc)_2$ (3 mol% of Pd in both instances). The relative intensity of tetramer **4a** over time is also presented for these two catalytic systems (see also Figure S5 for a representation including trimer **5a**). Importantly, the similarity of the plots indicates that the catalytically active species produced from Pd@MIL-101-NH_2(Cr) are essentially the same as those formed from $Pd(OAc)_2$. Tetramer **4a** builds up quickly at the start of the reaction, reaching a maximum concentration at t = 30 min when the yield of **3a** is already close to 80%. After this time, the concentration of these oxidative-addition Pd species quickly diminishes as the concentration of bromide **1a** depletes, and the yield of **3a** reaches 94% (t = 55 min). From this point, the yield of **3a** remains essentially constant, and the oxidative-addition intermediates reach a steady state. The fact that the yield of **3a** does not progress further to >99%, and that the relative intensity of **4a** remains constant, indicates a lack of boronic acid available to use in the transmetalation step. To test this hypothesis, additional boronic acid **2a** (1 equiv.) and potassium fluoride (2 equiv.) were added to the reaction mixture at t = 125 min, and the reaction was monitored until t = 135 min. We observed then that oxidative-addition intermediate **4a** was fully consumed, and at the same time the yield of **3a** increased to >99%. Although this indicates that the oxidative-addition tetramers are consumed upon reaction with boronic acid **2a**, at this point we could not distinguish whether a direct transmetalation from **4a** occurs or, alternatively, a breakdown into an oxidative-addition monomer is promoted upon reaction with the boronic acid. We therefore turned to density functional theory (DFT) calculations to try to understand the reactivity of **4a** and **7a**.

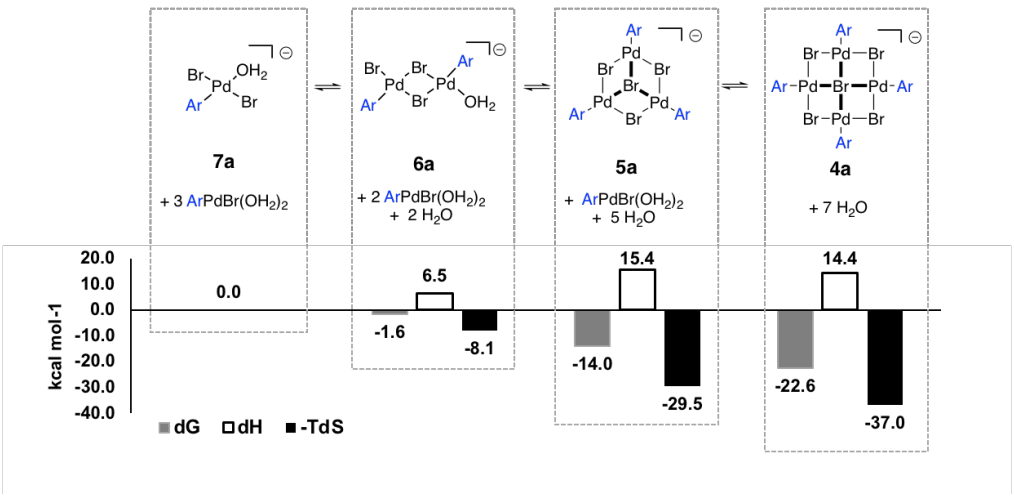

Figure 3. (a) Oligomerization of oxidative-addition intermediates and Gibbs free-energy change for the equilibrium species involved in the formation of tetramer **4a**. Optimized structures for monomeric and dimeric oxidative-addition intermediates found by MS (note that for both monomer and dimer, H_2O has been considered for coordinatively saturated Pd centers). Ar = $C_6H_4CF_3$.

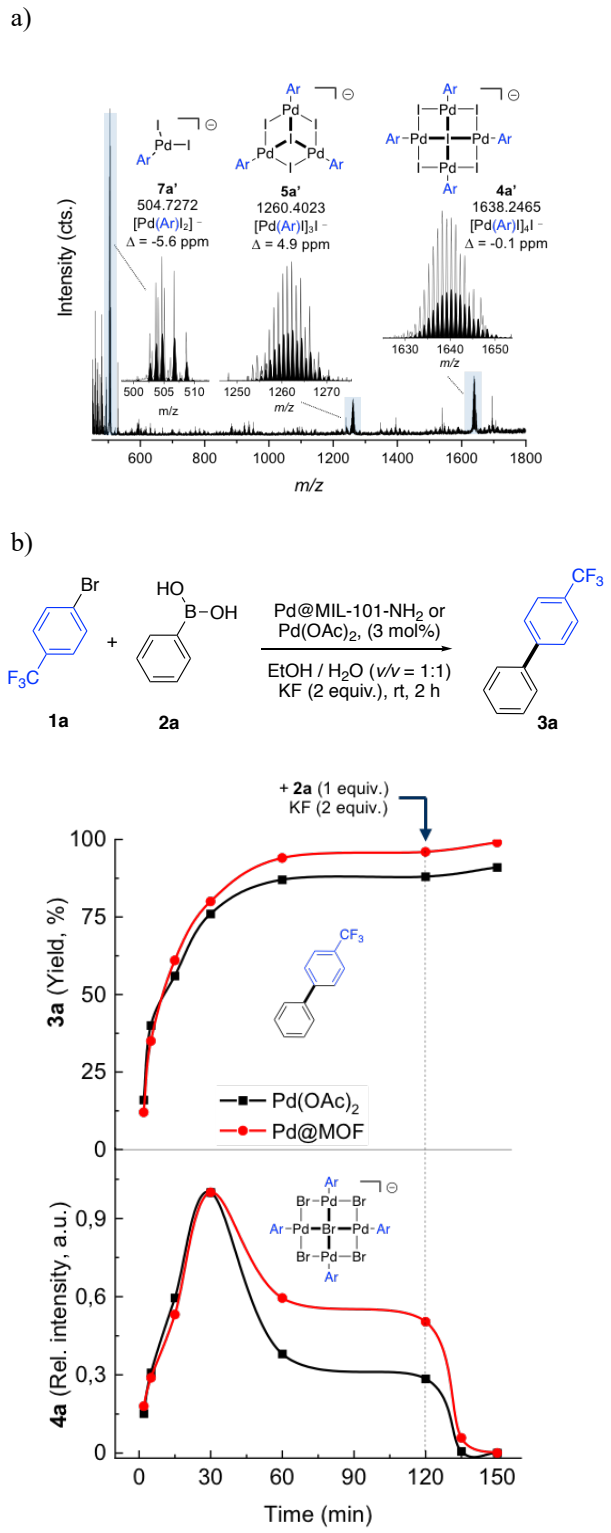

Figure 4. (a) Identified adducts in filtrate B, indicating measured mass (monoisotopic), formula, and error; (b) Monitoring of the intensity of **4a** by ESI(–)-MS and yield of **3a** over time. Yields were determined by ^{1}H NMR spectroscopy using 1,3,5-trimethoxybenzene as an internal standard.

The computational study of the transmetalation step started by studying the reaction of tetramer **4a** with fluorodihydroxy(phenyl)borate (**8a**) (Figure 6). Fluoroborates are formed under the reaction conditions when fluoride salts are used as the base.[75] In the initial step of the transmetalation, borate **8a** enters from below the plane of the four palladium atoms and coordinates to one of the four Pd centers, forming a Pd–O bond, with concomitant breaking of Pd–Br bond to the central bromide. Since this central bromide in **4a** was coordinated to three additional Pd centers, the bond-breaking step is very easy, and has a low activation free energy of 7.9 kcal/mol, and a reaction free energy of –1.0 kcal/mol (**Int1**). Next, a π-phenyl interaction replaces the second Pd–Br bond, through another very easy process with an activation free energy of only 1.9 kcal/mol, and a reaction free energy of –2.0 kcal/mol (**Int2**). Now the tetramer is set for the actual transmetalation step, where the Pd–C σ bond is formed (**Int3**). The barrier is very low, only 10.0 kcal/mol relative to the reacting intermediate. The very low trans influence of the bridging bromide is probably facilitating the formation of the Pd–C bond, and the reaction is very exergonic, leading to a tetramer with one of the Pd(II) species bearing two aryl groups. In this same step, $BF(OH)_2$ spontaneously decoordinates from Pd, and is replaced by a Pd–Br bond. Overall, all the steps involved in the transmetalation process were found to be very easy. This might be because no strong bonds in the palladium cluster need to be broken. As the Pd–Br interaction decreases at the reacting palladium center, the remaining Pd–Br interactions are strengthened at the spectator Pd sites, leading to very low activation energies. As tetramer **4a** has an unfavorable enthalpy of formation (Figure 3b), it is very susceptible to react, but it still forms in substantial amounts due to the entropic increase in its formation. The fact that it is possible for this tetramer to form relies on the coordination features of halides, and the absence of other stronger donor ligands (*vide infra*). Phosphines and carbenes interact strongly with palladium, and thus minimize its aggregation. However, the formation of reactive palladium intermediates from complexes bearing these ligands requires ligand-dissociation steps that in some cases can be rate determining.[76,77] Reductive elimination of two aryl groups from Pd(II) is usually a straightforward process, and also here we find low activation energies of only 11.6 kcal/mol leading to a Pd(0) species with the product coordinated (**Int4**).

The oxidative addition of 1-bromo-4-(trifluoromethyl)benzene (**1a**) to **Int4**, regenerating tetramer **4a**, was then investigated. Replacing the π-coordinated biaryl **3a** by aryl bromide **1a** was found to be slightly exergonic (6.5 kcal/mol). Oxidative addition then proceeds with a very low activation free energy of 0.5 kcal/mol to regenerate tetramer **4a**. The very low oxidative-addition barrier is probably due to the very bare Pd atom, where the only two ligands other than **1a** are the bridging bromides. This limited stabilization of the Pd(0) leads to very high reactivity towards the reactant, but could also lead to rapid aggregation and the formation of larger Pd(0) clusters. We also calculated the transmetalation from a monomeric palladium species (**7a**), which resulted in an activation energy of 25.8 kcal/mol. This result indicates that it is significantly more favorable for tetramer **4a** to undergo transmetalation than for monomer **7a** (Figure S6).

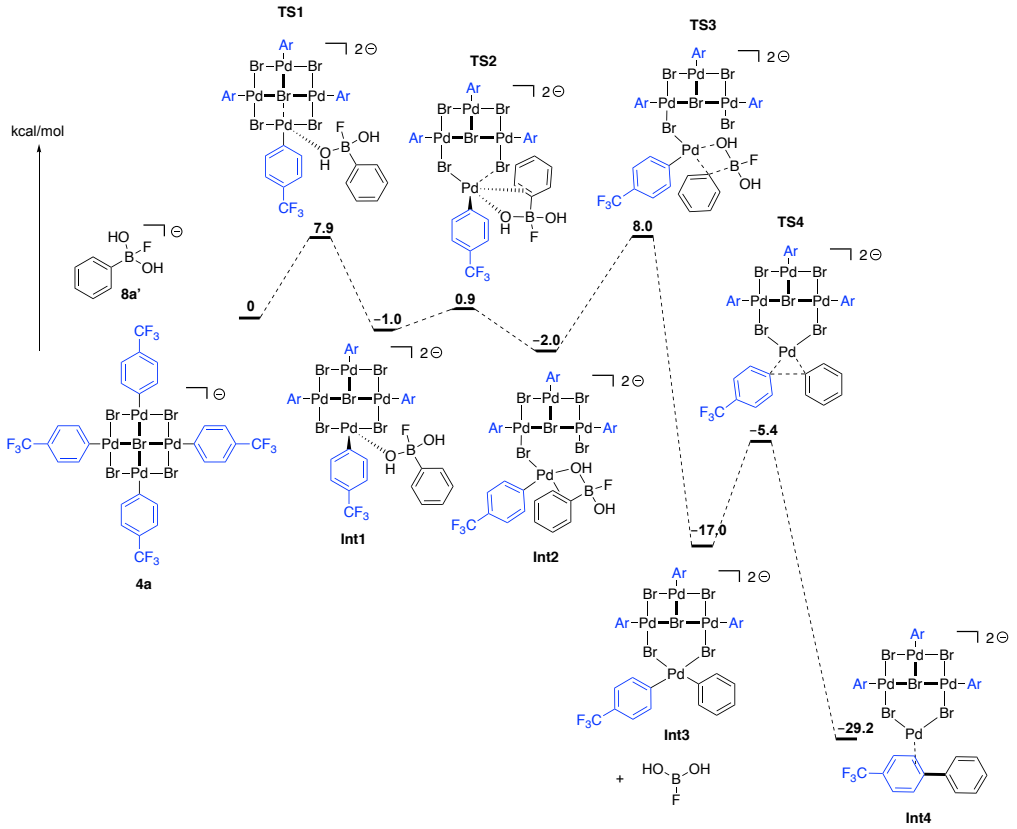

Figure 6. Free energy profile for the transmetalation and reductive elimination steps from **4a**.

Oxidative-addition tetramer **4a** was also observed by ESI(−)-MS when *p*-fluorophenylboronic acid (**2b**) was used. On the other hand, the nature of the aryl bromide **1a** significantly influences the formation of tetrameric intermediates **4**. Only aryl bromides with electron-withdrawing groups (EWG), such as **1a** (R = CF_3), **1b** (R = F), **1c** (R = SF_5), **1d** (R = OCF_3), **1e** (R = SCF_3), and **1f** (R = SO_2CF_3) led to the formation of tetramers (**4a**–**4f**), as observed by ESI(−)-MS (Figures 7 and Figure S7). With non-electron-poor aryl bromides, such as **1g** (R = H), **1h** (R = Me), and **1i** (R = OMe), species **4** were not detected (Figure 7). The stability of tetrameric oxidative-addition intermediates containing electron-donating groups (EDGs) was assessed by DFT calculations. The results showed that the formation of these species is still thermodynamically favored, however they are less stable than those containing EWGs. Replacement of the CF_3 groups on the aryl group with CH_3 led to a change from −22.6 kcal/mol for the formation of the tetramer (as shown in Figure 3) to −15.7 kcal/mol. Note that the free-energy calculation assumes the reference state to be one $[PdBr_2Ar(OH_2)]^-$ and three $PdBrAr(OH_2)_2$, but the reaction mixture may actually contain more species that affect the equilibria. However, the difference between the aryl groups with EWG or EDG is probably due to the difference in stability of the respective tetramers. This difference in stability may explain why the adducts containing EDGs could not be detected by ESI(−)-MS.

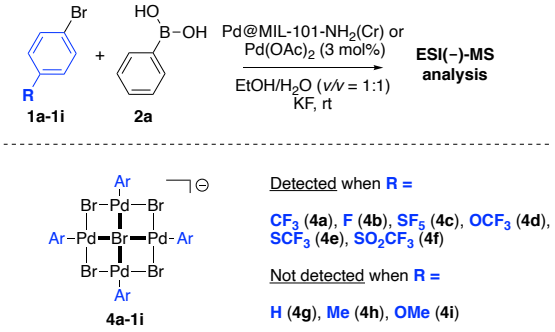

Figure 7. Pd(II) anionic oxidative-addition tetramers from diverse aryl bromides.

We carried out *in situ* ^{19}F NMR spectroscopy studies[78,79] with $Pd(OAc)_2$ as the catalyst to avoid the use of the insoluble MOF (Figures 8 and Figure S8). We used a Pd loading of 10 mol% in these experiments so that we would be able to detect palladium intermediates. Besides the expected signals for aryl halide **1a** (−62.72 ppm) and product **3a** (−62.36 ppm), three signals for CF_3-containing species were observed: **I** (singlet, −61.45 ppm), **II** (broad singlet, −61.11 ppm), and **III** (transient broad singlet, −60.41 → −60.94 ppm) (Figure 8a). The transient band **III** showed a rather constant intensity over time, reaching a steady state at ca. 93 min (Figure S9) when the yield of **3a** was 76%. Bands **I** and **II** showed significantly higher intensities than band **III**, both

reaching their maximum intensities at ca. 93 min (**I**/**II**/**III** = 0.9/1/0.1, Figure 8a and Figure S9). The intensity of band **I** over time is rather similar to that of band **II** over time (Figure S9). At t = 373 min, further boronic acid **2a** (1 equiv.) and base (1 equiv.) were added to the NMR tube. This resulted in a rapid fading of bands **I** and **II**, while the chemical shift of band **III** moved from −60.94 to −60.41 ppm (Figure 8b, black solid arrows). From the ESI(−)-MS analysis (Figure 5), we determined that tetramer **4a** was consumed when boronic acid **2a** and base were added. As bands **I** and **II** also faded away when these reagents were added, this indicates that these bands may correspond to oxidative-addition intermediates. To test this idea, we compared the reaction profile of tetramer **4a** as determined in Figure 4b (black squares, cat = $Pd(OAc)_2$) with the combined intensities of bands **I** and **II** over time, obtained from the ^{19}F NMR experiments, also using $Pd(OAc)_2$. As the conditions were different in these two experiments (i.e., reaction flask *vs* NMR tube, stirring rate, and catalyst loading), we have plotted the normalized intensities of **4a** (ESI) and that of bands **I** + **II** (NMR) *vs* a normalized time-scale (t/t_{max}) for each experiment (Figure 8c). The correlation of the intensities along the reaction profile is excellent, and thus we can assign bands **I** and **II** as oxidative-addition intermediates. The correlation is also excellent when the intensities of band **I** and band **II** are considered separately (Figure S10). Note that the evolution of the yield of **3a** in the NMR and ESI experiments correspond very well with each other across the normalized timescale (Figure 8a). The structures of the species responsible for bands **I** and **II** cannot be fully elucidated, but probably these bands correspond to tetramer **4a** and a related oxidative-addition species. The latter might be a species where a bromide bond has been substituted by a water ligand, which may well occur under the conditions of the NMR experiment. This assignment is also supported by the rapid fading of the two bands after the addition of boronic acid (min 373, Figure 8b). When 1 equiv. of aryl bromide **1a** was added (t = 418 min), bands **I** and **II** reappeared (Figure 8b, blue arrows), which further reinforces the assignment. Elucidation of the identity of the species responsible for band **III** is more difficult, as this band is probably due to a number of interconverting palladium species.

This study provides insights into the mechanism of the Suzuki–Miyaura cross-coupling reaction catalyzed by Pd nanoparticles immobilized into MIL-101-NH_2(Cr). The excellent activity of this heterogeneous catalyst in the coupling of aryl bromides with boronic acids can be explained by the formation of tetrameric oxidative-addition palladium(II) intermediates. These species were observed by electrospray ionization high-resolution mass spectroscopy in the negative mode in the coupling of electron-poor aryl bromides with boronic acids. The weak bonding in the tetrameric oxidative-addition species allows an easy transmetalation at room temperature (activation energy 10.0 kcal/mol); in contrast, the activation energy for the corresponding reaction with an oxidative-addition monomer was significantly higher (25.8 kcal/mol. Aryl iodides also give rise to tetrameric palladium adducts. However, the formation of stable off-cycle palladium iodide salts, such as $[Pd_2I_4]_n^-$, results in much lower catalytic efficiencies than those obtained with aryl bromides.

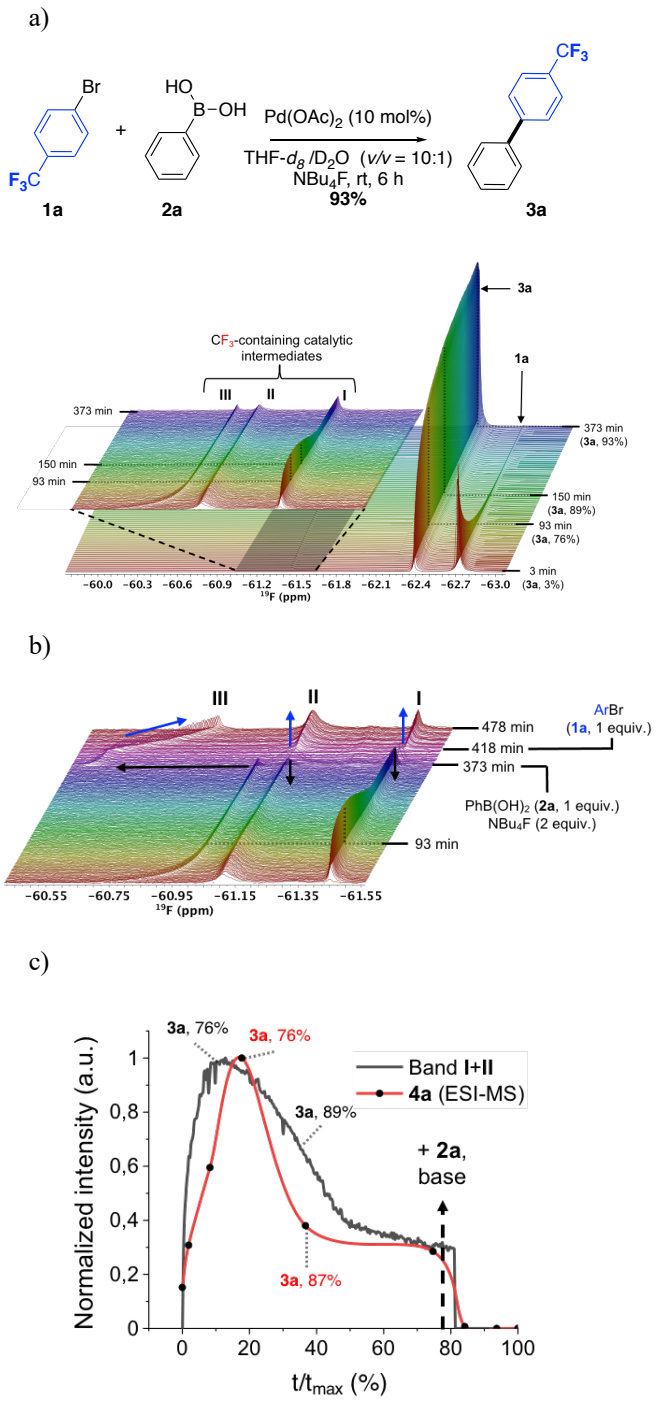

Figure 8. (a) Real-time ^{19}F NMR spectra. Inset shows the signals for catalytic intermediates between −60.6 and −61.6 ppm, using 1,4-difluorobenzene as an internal standard (−120.00 ppm); (b) ^{19}F NMR addition experiments and monitoring of catalytic intermediates; (c) Correlation between the intensity of **4a** (ESI-MS) and the intensity of bands **I** and **II**, plotted against reaction progress.

The same tetrameric species have been observed in this work when using $Pd(OAc)_2$, which leads us to conclude that Pd@MIL-101-NH_2(Cr) behaves as a reservoir of very active ligandless catalytically active species. The advantage of using Pd@MIL-101-NH_2(Cr) *vs.* $Pd(OAc)_2$ is that in the former case, the catalyst can be filtered off and reused.[56] When using $Pd(OAc)_2$, the catalyst cannot be recycled, resulting in

a significantly higher consumption of palladium. Thus, the synthetic efforts needed to prepare Pd@MOF catalysts can be fully justified. In "cocktail"-type systems, multiple mechanistic pathways are possible, and the electronic properties of the substrates may determine which pathway is favored in any particular case. This work suggests that tetrameric oxidative-addition palladium(II) species can provide a reaction pathway that proceeds *via* a very facile transmetallation step, usually the rate-limiting step in Suzuki-Miyaura cross-couplings.

ASSOCIATED CONTENT

Supporting Information

General methods, STEM images, ^{19}F NMR and computational data.

AUTHOR INFORMATION

Corresponding Author

Prof. Belén Martín-Matute – belen.martin.matute@su.se

ACKNOWLEDGMENT

The authors are grateful for support from the Knut and Alice Wallenberg Foundation (KAW 2016.0072), from the Swedish Research Council through Vetenskapsrådet, from the Göran Gustafsson Foundation, and from the Swedish Foundation for Strategic Environmental Research (MistraSafeChem, project number 2018/11). This work was performed, in part, at the Electron Microscopy Centre, supported by the Department of Materials and Environmental Chemistry and Faculty of Science at Stockholm University, Sweden. We thank Prof. J.-E. Bäckvall for helpful discussions.

REFERENCES

(1) Miyaura, N.; Suzuki, A. Stereoselective Synthesis of Arylated (E)-Alkenes by the Reaction of Alk-1-Enylboranes with Aryl Halides in the Presence of Palladium Catalyst. *J. Chem. Soc. Chem. Commun.* **1979**, 866.

(2) Miyaura, N.; Suzuki, A. Palladium-Catalyzed Cross-Coupling Reactions of Organoboron Compounds. *Chem. Rev.* **1995**, *95*, 2457–2483.

(3) Hooshmand, S. E.; Heidari, B.; Sedghi, R.; Varma, R. S. Recent Advances in the Suzuki-Miyaura Cross-Coupling Reaction Using Efficient Catalysts in Eco-Friendly Media. *Green Chem.* **2019**, *21*, 381–405.

(4) Beletskaya, I. P.; Alonso, F.; Tyurin, V. The Suzuki-Miyaura Reaction after the Nobel Prize. *Coord. Chem. Rev.* **2019**, *385*, 137–173.

(5) Schmidt, A. F.; Kurokhtina, A. A.; Larina, E. V. Role of a Base in Suzuki-Miyaura Reaction. *Russ. J. Gen. Chem.* **2011**, *81*, 1573–1574.

(6) Carrow, B. P.; Hartwig, J. F. Distinguishing between Pathways for Transmetalation in Suzuki-Miyaura Reactions. *J. Am. Chem. Soc.* **2011**, *133*, 2116–2119.

(7) Amatore, C.; Le Duc, G.; Jutand, A. Mechanism of Palladium-Catalyzed Suzuki-Miyaura Reactions: Multiple and Antagonistic Roles of Anionic "Bases" and Their Countercations. *Chem. Eur. J.* **2013**, *19*, 10082–10093.

(8) Amatore, C.; Jutand, A.; Leduc, G. The Triple Role of Fluoride Ions in Palladium-Catalyzed Suzuki-Miyaura Reactions: Unprecedented Transmetalation from [ArPdFL 2] Complexes. *Angew. Chem. Int. Ed.* **2012**, *51*, 1379–1382.

(9) Amatore, C.; Jutand, A.; Le Duc, G. Kinetic Data for the Transmetalation/Reductive Elimination in Palladium-Catalyzed Suzuki-Miyaura Reactions: Unexpected Triple Role of Hydroxide Ions Used as Base. *Chem. Eur. J.* **2011**, *17*, 2492–2503.

(10) Amatore, C.; Jutand, A.; Le Duc, G. Mechanistic Origin of Antagonist Effects of Usual Anionic Bases (OH -, CO 32-) as Modulated by Their Countercations (Na +, Cs +, K +) in Palladium-Catalyzed Suzuki-Miyaura Reactions. *Chem. Eur. J.* **2012**, *18*, 6616–6625.

(11) Thomas, A. A.; Denmark, S. E. Pre-Transmetalation Intermediates in the Suzuki-Miyaura Reaction Revealed: The Missing Link. *Science* **2016**, *352*, 329–332.

(12) Olding, A.; Ho, C.; Canty, A.; Lucas, N.; Horne, J.; Bissember, A. C. Synthesis of Arylpalladium(II) Boronates: Confirming the Structure of Pre-transmetalation Intermediates in the Suzuki–Miyaura Reaction Crystallographically. *Angew. Chem. Int. Ed.* **2021**, anie.202104802.

(13) Fu, F.; Xiang, J.; Cheng, H.; Cheng, L.; Chong, H.; Wang, S.; Li, P.; Wei, S.; Zhu, M.; Li, Y. A Robust and Efficient Pd3 Cluster Catalyst for the Suzuki Reaction and Its Odd Mechanism. *ACS Catal.* **2017**, *7*, 1860–1867.

(14) Schoenebeck, F.; Houk, K. N. Ligand-Controlled Regioselectivity in Palladium-Catalyzed Cross Coupling Reactions. *J. Am. Chem. Soc.* **2010**, *132*, 2496–2497.

(15) Albéniz, A. C.; Casado, A. L.; Espinet, P. O- and m-(Bromotetrafluorophenyl)Palladium(II) Complexes: Atropisomerism Studies by 19F NMR and Measurement of through-Space F-F Coupling Constants. *Organometallics* **1997**, *16*, 5416–5423.

(16) Liu, C.; Zhang, Y.; Liu, N.; Qiu, J. A Simple and Efficient Approach for the Palladium-Catalyzed Ligand-Free Suzuki Reaction in Water. *Green Chem.* **2012**, *14*, 2999–3003.

(17) Biffis, A.; Centomo, P.; Del Zotto, A.; Zecca, M. Pd Metal Catalysts for Cross-Couplings and Related Reactions in the 21st Century: A Critical Review. *Chem. Rev.* **2018**, *118*, 2249–2295.

(18) Alimardanov, A.; Schmieder-Van De Vondervoort, L.; De Vries, A. H. M.; De Vries, J. G. Use of "Homeopathic" Ligand-Free Palladium as Catalyst for Aryl-Aryl Coupling Reactions. *Adv. Synth. Catal.* **2004**, *346*, 1812–1817.

(19) Alonso, D. A.; Nájera, C.; Pacheco, M. C. Highly Active Oxime-Derived Palladacycle Complexes for Suzuki-Miyaura and Ullmann-Type Coupling Reactions. *J. Org. Chem.* **2002**, *67*, 5588–5594.

(20) Han, W.; Liu, C.; Jin, Z. Aerobic Ligand-Free Suzuki Coupling Reaction of Aryl Chlorides Catalyzed by in Situ Generated Palladium Nanoparticles at Room Temperature. *Adv. Synth. Catal.* **2008**, *350*, 501–508.

(21) Boruah, P. R.; Ali, A. A.; Saikia, B.; Sarma, D. A Novel Green Protocol for Ligand Free Suzuki-Miyaura Cross-Coupling Reactions in WEB at Room Temperature. *Green Chem.* **2015**, *17*, 1442–1445.

(22) Xu, L.; Liu, F. Y.; Zhang, Q.; Chang, W. J.; Liu, Z. L.; Lv, Y.; Yu, H. Z.; Xu, J.; Dai, J. J.; Xu, H. J. The Amine-Catalysed Suzuki–Miyaura-Type Coupling of Aryl Halides and Arylboronic Acids. *Nat. Catal.* **2021**, *4*, 71–78.

(23) Avanthay, M.; Bedford, R.; Begg, C.; Böse, D.; Clayden, J.; Davis, S.; Eloi, J.C.; Goryunov, G.P.; Hartung, I.V.; Heeley, J.; Khaikin, K.A.; Kitching, M.; Krieger, J.; Kulyabin, P.S.; Lennox, A.; Nolla-Saltiel, R.; Pridmore, N.E.; Rowsell, B.J.S.; Sparkes, H. J. Amine-Catalysed Suzuki–Miyaura-Type Coupling? The Identification and Isolation of the Palladium Culprits. *ChemRxiv* **2021**.

(24) Novák, Z.; Adamik, R.; Csenki, J. T.; Béke, F.; Gavaldik, R. Curse or Blessing ? Influence of Impurities on Cross-Coupling — Guideline for Elucidating Catalysts. *ChemRxiv* **2021**, 1–17.

(25) Diallo, A. K.; Ornelas, C.; Salmon, L.; Aranzaes, J. R.; Astruc, D. "Homeopathic" Catalytic Activity and Atom-Leaching Mechanism in Miyaura-Suzuki Reactions under Ambient Conditions with Precise Dendrimer-Stabilized Pd Nanoparticles. *Angew. Chem. Int. Ed.* **2007**, *46*, 8644–8648.

(26) Yang, Q.; Xu, Q.; Jiang, H. L. Metal-Organic Frameworks Meet Metal Nanoparticles: Synergistic Effect for Enhanced Catalysis. *Chem. Soc. Rev.* **2017**, *46*, 4774–4808.

(27) Van Velthoven, N.; Waitschat, S.; Chavan, S. M.; Liu, P.; Smolders, S.; Vercammen, J.; Bueken, B.; Bals, S.; Lillerud, K. P.; Stock, N.; De Vos, D. E. Single-Site Metal-Organic Framework Catalysts for the Oxidative Coupling of Arenes: Via

C-H/C-H Activation. *Chem. Sci.* **2019**, *10*, 3616–3622.
(28) Van Velthoven, N.; Wang, Y.; Van Hees, H.; Henrion, M.; Bugaev, A. L.; Gracy, G.; Amro, K.; Soldatov, A. V.; Alauzun, J. G.; Mutin, P. H.; De Vos, D. E. Heterogeneous Single-Site Catalysts for C-H Activation Reactions: Pd(II)-Loaded S,O-Functionalized Metal Oxide-Bisphosphonates. *ACS Appl. Mater. Interfaces* **2020**, *12*, 47457–47466.
(29) Jeffery, T. On the Efficiency of Tetraalkylammonium Salts in Heck Type Reactions. *Tetrahedron* **1996**, *52*, 10113–10130.
(30) Jeffery, T.; David, M. [Pd/Base/QX] Catalyst Systems for Directing Heck-Type Reactions. *Tetrahedron Lett.* **1998**, *39*, 5751–5754.
(31) Reetz, M. T.; Westermann, E.; Lohmer, R.; Lohmer, G. A Highly Active Phosphine-Free Catalyst System for Heck Reactions of Aryl Bromides. *Tetrahedron Lett.* **1998**, *39*, 8449–8452.
(32) Ananikov, V. P.; Beletskaya, I. P. Toward the Ideal Catalyst: From Atomic Centers to a "Cocktail" of Catalysts. *Organometallics* **2012**, *31*, 1595–1604.
(33) Kashin, A. S.; Ananikov, V. P. Catalytic C-C and C-Heteroatom Bond Formation Reactions: In Situ Generated or Preformed Catalysts? Complicated Mechanistic Picture behind Well-Known Experimental Procedures. *J. Org. Chem.* **2013**, *78*, 11117–11125.
(34) Adrio, L. A.; Nguyen, B. N.; Guilera, G.; Livingston, A. G.; Hii, K. K. Speciation of Pd(OAc)2 in Ligandless Suzuki-Miyaura Reactions. *Catal. Sci. Technol.* **2012**, *2*, 316–323.
(35) Crabtree, R. H. Resolving Heterogeneity Problems and Impurity Artifacts in Operationally Homogeneous Transition Metal Catalysts. *Chem. Rev.* **2012**, *112*, 1536–1554.
(36) Schmidt, A. F.; Kurokhtina, A. A. Distinguishing between the Homogeneous and Heterogeneous Mechanisms of Catalysis in the Mizoroki-Heck and Suzuki-Miyaura Reactions: Problems and Prospects. *Kinet. Catal.* **2012**, *53*, 714–730.
(37) Zhao, Y.; Du, L.; Li, H.; Xie, W.; Chen, J. Is the Suzuki-Miyaura Cross-Coupling Reaction in the Presence of Pd Nanoparticles Heterogeneously or Homogeneously Catalyzed? An Interfacial Surface-Enhanced Raman Spectroscopy Study. *J. Phys. Chem. Lett.* **2019**, *10*, 1286–1291.
(38) Ellis, P. J.; Fairlamb, I. J. S.; Hackett, S. F. J.; Wilson, K.; Lee, A. F. Evidence for the Surface-Catalyzed Suzuki-Miyaura Reaction over Palladium Nanoparticles: An Operando XAS Study. *Angew. Chem. Int. Ed.* **2010**, *49*, 1820–1824.
(39) Leyva-Pérez, A.; Oliver-Meseguer, J.; Rubio-Marqués, P.; Corma, A. Water-Stabilized Three- and Four-Atom Palladium Clusters as Highly Active Catalytic Species in Ligand-Free C-C Cross-Coupling Reactions. *Angew. Chem. Int. Ed.* **2013**, *52*, 11554–11559.
(40) Polynski, M. V.; Ananikov, V. P. Modeling Key Pathways Proposed for the Formation and Evolution of "Cocktail"-Type Systems in Pd-Catalyzed Reactions Involving ArX Reagents. *ACS Catal.* **2019**, *9*, 3991–4005.
(41) Lennox, A. J. J.; Lloyd-Jones, G. C. Transmetalation in the Suzuki-Miyaura Coupling: The Fork in the Trail. *Angew. Chem. Int. Ed.* **2013**, *52*, 7362–7370.
(42) Phan, N. T. S.; Van Der Sluys, M.; Jones, C. W. On the Nature of the Active Species in Palladium Catalyzed Mizoroki-Heck and Suzuki-Miyaura Couplings - Homogeneous or Heterogeneous Catalysis, a Critical Review. *Adv. Synth. Catal.* **2006**, *348*, 609–679.
(43) Mpungose, P. P.; Vundla, Z. P.; Maguire, G. E. M.; Friedrich, H. B. The Current Status of Heterogeneous Palladium Catalysed Heck and Suzuki Cross-Coupling Reactions. *Molecules* **2018**, *23*, 1–24.
(44) Carrow, B. P.; Hartwig, J. F. Ligandless, Anionic, Arylpalladium Halide Intermediates in the Heck Reaction. *J. Am. Chem. Soc.* **2010**, *132*, 79–81.
(45) Evans, J.; O'Neill, L.; Kambhampati, V. L.; Rayner, G.; Turin, S.; Genge, A.; Dent, A. J.; Neisius, T. Structural Characterisation of Solution Species Implicated in the Palladium-Catalysed Heck Reaction by Pd K-Edge X-Ray Absorption Spectroscopy: Palladium Acetate as a Catalyst Precursor. *J. Chem. Soc. Dalt. Trans.* **2002**, No. 10, 2207–2212.
(46) Yang, Q.; Yao, F.; Zhong, Y.; Chen, F.; Shu, X.; Sun, J.; He, L.; Wu, B.; Hou, K.; Wang, D.; Li, X. Metal–Organic Framework Supported Palladium Nanoparticles: Applications and Mechanisms. *Part. Part. Syst. Charact.* **2019**, *36*, 1–19.
(47) Luo, S.; Zeng, Z.; Zeng, G.; Liu, Z.; Xiao, R.; Chen, M.; Tang, L.; Tang, W.; Lai, C.; Cheng, M.; Shao, B.; Liang, Q.; Wang, H.; Jiang, D. Metal Organic Frameworks as Robust Host of Palladium Nanoparticles in Heterogeneous Catalysis: Synthesis, Application, and Prospect. *ACS Appl. Mater. Interfaces* **2019**, *11*, 32579–32598.
(48) Li, H.; Zhu, Z.; Zhang, F.; Xie, S.; Li, H.; Li, P.; Zhou, X. Palladium Nanoparticles Confined in the Cages of MIL-101: An Efficient Catalyst for the One-Pot Indole Synthesis in Water. *ACS Catal.* **2011**, *1*, 1604–1612.
(49) Wang, Q.; Astruc, D. State of the Art and Prospects in Metal-Organic Framework (MOF)-Based and MOF-Derived Nanocatalysis. *Chem. Rev.* **2020**, *120*, 1438–1511.
(50) Chen, L.; Gao, Z.; Li, Y. Immobilization of Pd(II) on MOFs as a Highly Active Heterogeneous Catalyst for Suzuki-Miyaura and Ullmann-Type Coupling Reactions. *Catal. Today* **2015**, *245*, 122–128.
(51) Zhang, M.; Guan, J.; Zhang, B.; Su, D.; Williams, C. T.; Liang, C. Chemical Vapor Deposition of Pd(C 3H 5)(C 5H 5) to Synthesize Pd@MOF-5 Catalysts for Suzuki Coupling Reaction. *Catal. Letters* **2012**, *142*, 313–318.
(52) Saha, D.; Sen, R.; Maity, T.; Koner, S. Anchoring of Palladium onto Surface of Porous Metal-Organic Framework through Post-Synthesis Modification and Studies on Suzuki and Stille Coupling Reactions under Heterogeneous Condition. *Langmuir* **2013**, *29*, 3140–3151.
(53) Huang, Y.; Zheng, Z.; Liu, T.; Lü, J.; Lin, Z.; Li, H.; Cao, R. Palladium Nanoparticles Supported on Amino Functionalized Metal-Organic Frameworks as Highly Active Catalysts for the Suzuki-Miyaura Cross-Coupling Reaction. *Catal. Commun.* **2011**, *14*, 27–31.
(54) Yuan, B.; Pan, Y.; Li, Y.; Yin, B.; Jiang, H. A Highly Active Heterogeneous Palladium Catalyst for the Suzuki-Miyaura and Ullmann Coupling Reactions of Aryl Chlorides in Aqueous Media. *Angew. Chem. Int. Ed.* **2010**, *49*, 4054–4058.
(55) Pascanu, V.; Hansen, P. R.; Bermejo Gómez, A.; Ayats, C.; Platero-Prats, A. E.; Johansson, M. J.; Pericàs, M.; Martín-Matute, B. Highly Functionalized Biaryls via Suzuki-Miyaura Cross-Coupling Catalyzed by Pd@MOF under Batch and Continuous Flow Regimes. *ChemSusChem* **2015**, *8*, 123–130.
(56) Pascanu, V.; Yao, Q.; Bermejo Gõmez, A.; Gustafsson, M.; Yun, Y.; Wan, W.; Samain, L.; Zou, X.; Martín-Matute, B. Sustainable Catalysis: Rational Pd Loading on MIL-101Cr-NH2 for More Efficient and Recyclable Suzuki-Miyaura Reactions. *Chem. Eur. J.* **2013**, *19*, 17483–17493.
(57) Verho, O.; Nagendiran, A.; Johnston, E. V.; Tai, C. W.; Bäckvall, J. E. Nanopalladium on Amino-Functionalized Mesocellular Foam: An Efficient Catalyst for Suzuki Reactions and Transfer Hydrogenations. *ChemCatChem* **2013**, *5*, 612–618.
(58) Tao, X.; Long, R.; Wu, D.; Hu, Y.; Qiu, G.; Qi, Z.; Li, B.; Jiang, R.; Xiong, Y. Anchoring Positively Charged Pd Single Atoms in Ordered Porous Ceria to Boost Catalytic Activity and Stability in Suzuki Coupling Reactions. *Small* **2020**, *16*, 1–11.
(59) Li, Y.; Xu, L.; Xu, B.; Mao, Z.; Xu, H.; Zhong, Y.; Zhang, L.; Wang, B.; Sui, X. Cellulose Sponge Supported Palladium Nanoparticles as Recyclable Cross-Coupling Catalysts. *ACS Appl. Mater. Interfaces* **2017**, *9*, 17155–17162.
(60) Wang, Y.; Liao, J.; Xie, Z.; Zhang, K.; Wu, Y.; Zuo, P.; Zhang, W.; Li, J.; Gao, Z. Zeolite-Enhanced Sustainable Pd-Catalyzed C-C Cross-Coupling Reaction: Controlled Release and Capture of Palladium. *ACS Appl. Mater. Interfaces* **2020**, *12*, 11419–11427.
(61) Song, K.; Liu, P.; Wang, J.; Tan, B.; Li, T. Highly Active Palladium Nanoparticles Immobilized on Knitting Microporous Organic Polymers as Efficient Catalysts for Suzuki–Miyaura Cross-Coupling Reaction. *J. Porous Mater.* **2016**, *23*, 725–731.
(62) Carson, F.; Pascanu, V.; Bermejo-Gómez, A.; Zhang, Y.; Platero-Prats, A. E.; Zou, X.; Martín-Matute, B. Influence of the Base on Pd@MIL-101-NH2(Cr) as Catalyst for the Suzuki-Miyaura Cross-Coupling Reaction. *Chem. Eur. J.* **2015**, *21*, 10896–10902.
(63) Galli, C.; Pau, T. The Dehalogenation Reaction of Organic Halides by Tributyltin Radical: The Energy of Activation vs. the BDE of the C-X Bond. *Tetrahedron* **1998**, *54*, 2893–2904.
(64) Belyakov, P. A.; Kadentsev, V. I.; Chizhov, A. O.; Kolotyrkina, N. G.; Shashkov, A. S.; Ananikov, V. P. Mechanistic Insight into Organic and Catalytic Reactions by Joint Studies Using Mass

Spectrometry and NMR Spectroscopy. *Mendeleev Commun.* **2010**, *20*, 125–131.
(65) Vikse, K. L.; McIndoe, J. S. Mechanistic Insights from Mass Spectrometry: Examination of the Elementary Steps of Catalytic Reactions in the Gas Phase. *Pure Appl. Chem.* **2015**, *87*, 361–377.
(66) Enquist, P. A.; Nilsson, P.; Sjöberg, P.; Larhed, M. ESI-MS Detection of Proposed Reaction Intermediates in the Air-Promoted and Ligand-Modulated Oxidative Heck Reaction. *J. Org. Chem.* **2006**, *71*, 8779–8786.
(67) Qian, R.; Liao, Y. X.; Guo, Y. L.; Guo, H. ESI-FTICR-MS Studies on Gas Phase Fragmentation Reactions of ArPd(PPh3)2I Complexes. *J. Am. Soc. Mass Spectrom.* **2006**, *17*, 1582–1589.
(68) Limberger, J.; Leal, B. C.; Monteiro, A. L.; Dupont, J. Charge-Tagged Ligands: Useful Tools for Immobilising Complexes and Detecting Reaction Species during Catalysis. *Chem. Sci.* **2015**, *6*, 77–94.
(69) Vikse, K. L.; Henderson, M. A.; Oliver, A. G.; McIndoe, J. S. Direct Observation of Key Intermediates by Negative-Ion Electrospray Ionisation Mass Spectrometry in Palladium-Catalysed Cross-Coupling. *Chem. Commun.* **2010**, *46*, 7412–7414.
(70) Yunker, L. P. E.; Ahmadi, Z.; Logan, J. R.; Wu, W.; Li, T.; Martindale, A.; Oliver, A. G.; McIndoe, J. S. Real-Time Mass Spectrometric Investigations into the Mechanism of the Suzuki-Miyaura Reaction. *Organometallics* **2018**, *37*, 4297–4308.
(71) Kolter, M.; Koszinowski, K. Second Comes First: Switching Elementary Steps in Palladium-Catalyzed Cross-Coupling Reactions. *Chem. Eur. J.* **2020**, *26*, 12212–12218.
(72) De Vries, J. G. A Unifying Mechanism for All High-Temperature Heck Reactions. the Role of Palladium Colloids and Anionic Species. *Dalt. Trans.* **2006**, No. 3, 421–429.
(73) Kashin, A. N.; Ganina, O. G.; Cheprakov, A. V.; Beletskaya, I. P. The Direct Non-Perturbing Leaching Test in the Phosphine-Free Suzuki-Miyaura Reaction Catalyzed by Palladium Nanoparticles. *ChemCatChem* **2015**, *7*, 2113–2121.
(74) Galushko, A. S.; Prima, D. O.; Burykina, J. V.; Ananikov, V. P. Comparative Study of Aryl Halides in Pd-Mediated Reactions: Key Factors beyond the Oxidative Addition Step. *Inorg. Chem. Front.* **2021**, *8*, 620–635.
(75) Lennox, A. J. J.; Lloyd-Jones, G. C. Selection of Boron Reagents for Suzuki-Miyaura Coupling. *Chem. Soc. Rev.* **2014**, *43*, 412–443.
(76) McMullin, C. L.; Fey, N.; Harvey, J. N. Computed Ligand Effects on the Oxidative Addition of Phenyl Halides to Phosphine Supported Palladium(0) Catalysts. *Dalt. Trans.* **2014**, *43*, 13545–13556.
(77) Barrios-Landeros, F.; Carrow, B. P.; Hartwig, J. F. Effect of Ligand Steric Properties and Halide Identity on the Mechanism for Oxidative Addition of Haloarenes to Trialkylphosphine Pd(0) Complexes. *J. Am. Chem. Soc.* **2009**, *131*, 8141–8154.
(78) Howe, P. W. A. Recent Developments in the Use of Fluorine NMR in Synthesis and Characterisation. *Prog. Nucl. Magn. Reson. Spectrosc.* **2020**, *118–119*, 1–9.
(79) Zientek, N.; Laurain, C.; Meyer, K.; Kraume, M.; Guthausen, G.; Maiwald, M. Simultaneous 19F-1H Medium Resolution NMR Spectroscopy for Online Reaction Monitoring. *J. Magn. Reson.* **2014**, *249*, 53–62.

Supplementary Information

Tetrameric Aryl Palladium Bromide Intermediates Leading to Facile Transmetalation in Suzuki–Miyaura Cross-Couplings with Pd@MIL-101-NH_2

Alejandro Valiente,[a] Cheuk-Wai Tai,[b] Mårten Ahlquist[c] and Belén Martín-Matute*,[a]

Belen.martin.matute@su.se

[a] Department of Organic Chemistry, Stockholm University, The Arrhenius Laboratory 16C, SE-106 91, Stockholm (Sweden)

[b] Department of Materials and Environmental Chemistry, Stockholm University, The Arrhenius Laboratory 16C, SE-106 91, Stockholm (Sweden)

[c] Department of Theoretical Chemistry and Biology,School of Engineering Sciences in Chemistry,Biotechnology and Health KTH Royal Institute of Technology SE-10691 Stockholm (Sweden)

Table of Contents

1. General information *2*

General Procedure for the Suzuki–Miyaura Reaction. 2

General Procedure for Filtration Tests. 2

ESI Mass Spectrometry 2

Computational details 3

General Procedure for the NMR Spectroscopy Experiments 3

Transmission Electron Microscopy 3

2. Supplementary figures *4*

3. References *11*

1. General information

Reagents and solvents were used as obtained from commercial suppliers. ICP-OES analysis was carried out by MEDAC Ltd (UK).

General Procedure for the Suzuki–Miyaura Reaction.

Pd@MIL-101-NH_2(Cr) **(**7.25 wt%; 4.4 mg, 0.009 mmol, 3 mol%), arylboronic acid (0.13 mmol, 1.4 equiv.), and KF (12 mg, 0.18 mmol, 2 equiv.) were added to a 4 mL glass vial. Then EtOH (50% aq. added together with the aryl halide (0.1 mmol), and the mixture was stirred (900 rpm) at room temperature. For kinetic profiles, the reactions were quenched at the desired times by the addition of HCl (1 M aq.; 300 μL).

General Procedure for Filtration Tests.

Filtration tests were carried out by filtering the whole reaction mixture (prepared as described in the general procedure above) at t_1 = 60 min using a filter (0.22 μm pore size). The filtrate was added to a new glass vial containing a second load of boronic acid, base, and aryl halide (no MOF was added). The mixture was stirred for a further 60 min (t_2), and the reaction was quenched as described above. The product yield was determined by ^{1}H NMR spectroscopy using 1,3,5-trimethoxybenzene as an internal standard, and the total amount of aryl halide added (0.2 mmol) as the limiting reagent.

ESI Mass Spectrometry

High-resolution mass spectra (HRMS) were recorded with a Bruker micrOTOF ESI-TOF mass spectrometer. Sample solutions were transferred into the ESI source with gastight syringes at flow rates of 180

μL/min, which was maintained by a syringe pump. The ESI source was operated with a voltage of +4000 V (HV end plate offset: −500 V) using N_2 as nebulizer (0.3 bar) and drying gas (4 L/min, temperature: 453 K). The experiments were typically carried out in negative mode ESI(−)-MS, with a scan range of *m/z* = 200–2000. Accuracies of <10 ppm were obtained for the measured *m/z* ratios after external calibration using a low concentration tuning mix solution (mixture of CF_3COOH and phosphazenes in H_2O/CH_3CN, Agilent Technologies). Theoretical exact *m/z* ratios and isotope patterns were calculated with the DataAnalysis software package (Bruker Daltonics).

Computational details

All computations were performed with the Jaguar program package by Schrödinger LLC.[1] All geometries were optimized using the dispersion corrected[2] B3LYP-D3 functional[3,4] with the LACVP** core potential[5] and basis set, which applies the 6-31G** basis set to all light elements. Solvation free energies were calculated using the PBF[6] solvation model for all palladium species with standard parameters for water solvation. Solvation free energies for all organic compounds were calculated using the SM8[7] model with the B3LYP-D3 functional and 6-31+G* basis set, which generates CM4 charges. The solvation free energy for water was -2.05 kcal mol-1 corresponding to the hydration free energy. Harmonic vibrational frequencies were calculated to assure that intermediates contained no imaginary frequencies and that transition states contained only one. Gibbs free energies for each species were calculated as the sum G = E(B3LYP-D3/LACV3P**++) + G_{solv} + ZPE + ΔH_{298} –TS, where a single point energy correction was made for each species with the larger LACV3P**++ basis set and core potential, and thermochemical parameters (ZPE = zero point vibrational energy, ΔH_{298} = contribution from excited vibrations at T = 298K and the pressure volume term pV, –TS = entropy at T = 298K). All solvation free energies were calculated at standard state at T = 298K.

General Procedure for the NMR Spectroscopy Experiments

^{19}F NMR spectra were recorded with a Bruker Avance III HD 500 MHz spectrometer equipped with a helium-cooled probe. ^{19}F chemical shifts (δ) are reported in ppm using 1,4-difluorobenzene (–120.00 ppm) as an internal standard. 32 scans per spectrum were collected at a scan rate of 1 second/scan. Typically, aryl halide (0.1 mmol), $NBu_4F\cdot(H_2O)_3$ (62 mg, 0.2 mmol, 2 equiv.) and the internal standard (0.1 mmol) were dissolved in the THF-d_8/D_2O mixture (10:1, *v/v*) in a 2 mL glass vial. The homogeneous solution was transferred into another vial containing the $Pd(OAc)_2$ precatalyst (2 mg, 0.01 mmol) and the boronic acid (0.14 mmol, 1.4 equiv.). As the reaction starts at room temperature, to avoid the loss in information between sample preparation and the start of the measurements, the mixture was immediately transferred into an NMR tube and cooled at –78 ºC until it was frozen. After this, the tube was placed into the NMR spectrometer, and the acquisitions were started while the sample slowly returned to 25 ºC and the reaction proceeded.

Transmission Electron Microscopy

Scanning Transmission Electron Microscopy (STEM) and energy dispersive x-ray spectroscopy study were performed on a Thermo Fischer aberration-corrected Themis Z microscope equipped with SuperX EDX system. The instrument was operated at 300 kV with a probe corrector (CEOS DCOR) corrected up to the fifth order. The electron probe with a convergence angle of 21.4 mrad and current of 100 pA was used. Bright-field (BF) and High-angle annular dark-field (HAADF) images and EDX spectra were acquired using Velox software (Thermo Fischer). MOF samples were placed on Cu TEM grids with holey carbon supporting films as dry powder. Reaction samples were dispersed on the TEM grids in the reaction solvent. Nanoparticle size analysis was carried out using ImageJ software. The reported values correspond to the average value of *ca.* 100 samples.

2.**Supplementary figures**

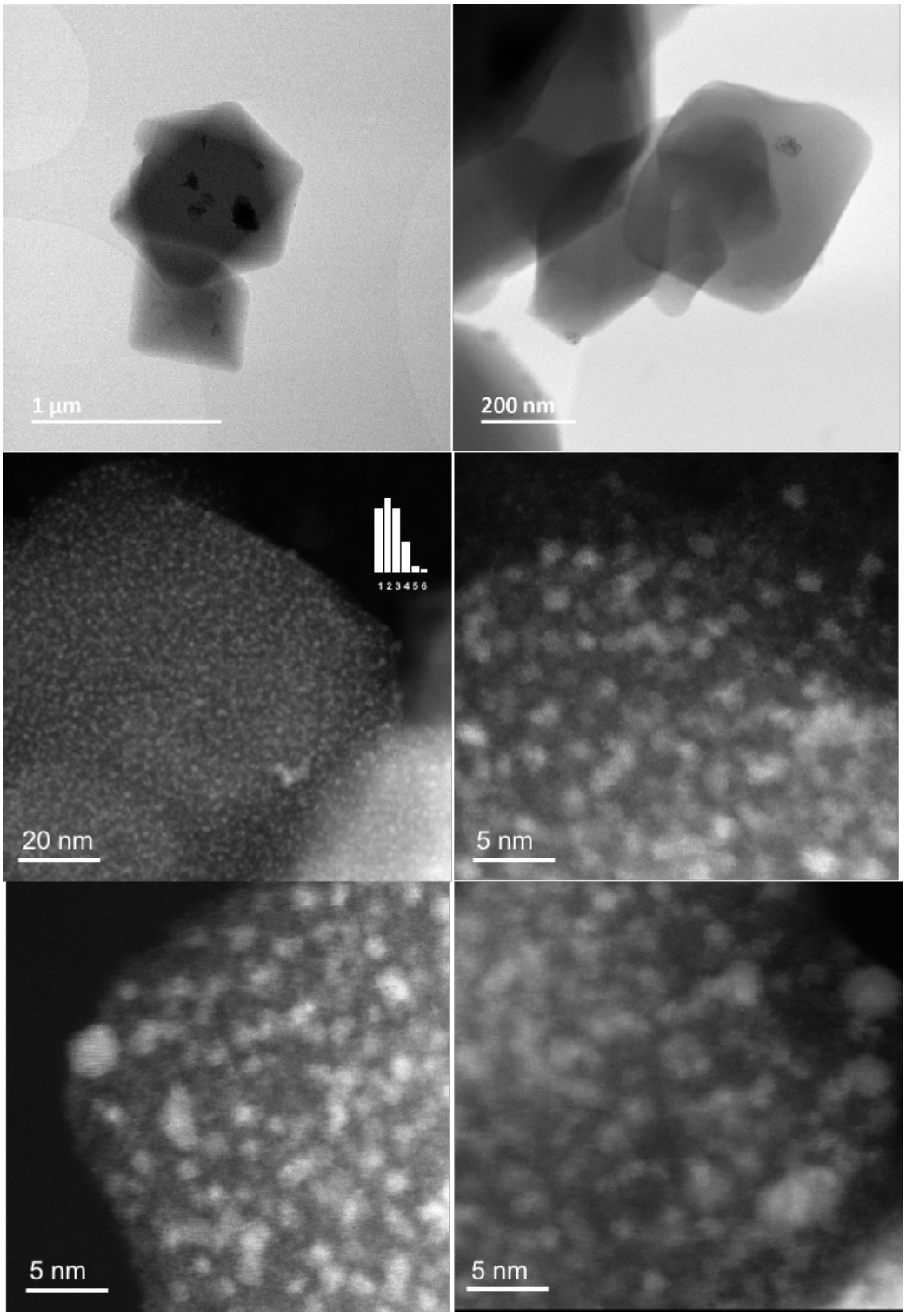

Figure S1. BF- and HAADF-STEM micrographs of Pd@MIL-101-NH_2

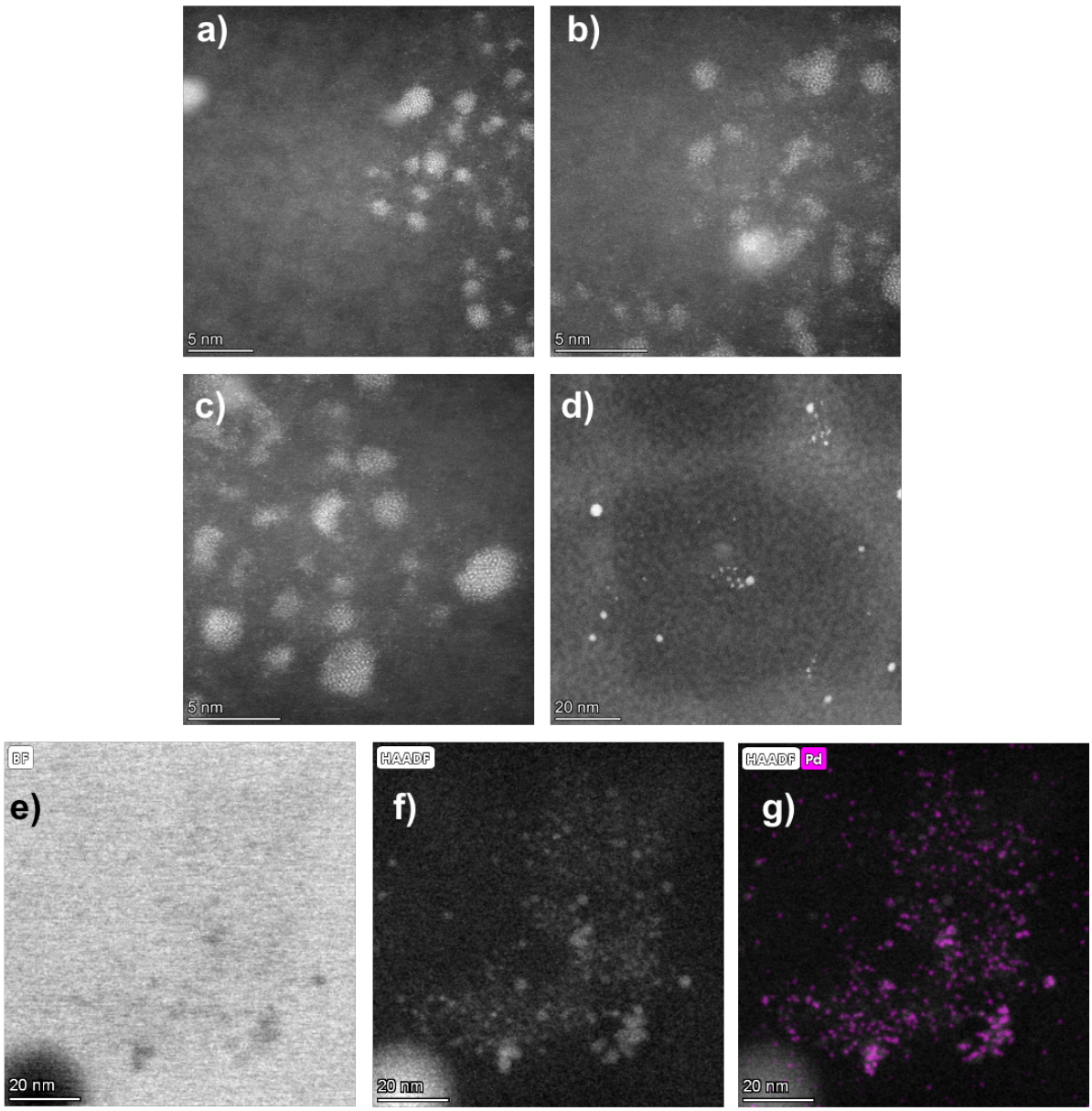

Figure S2. STEM micrographs of filtrate A: HAADF- (a – d, f); BF- (e) and EDX elemental mapping showing Pd (g).

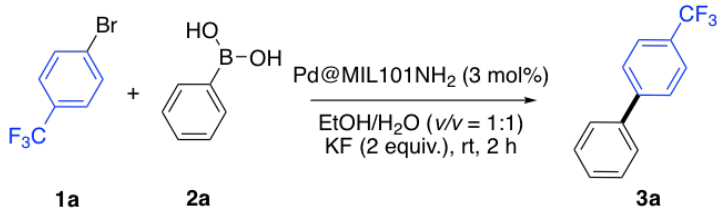

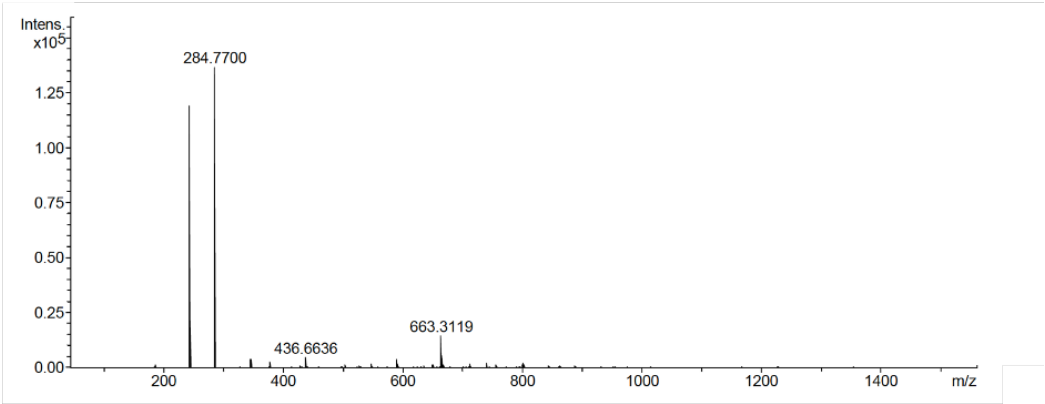

Figure S3. ESI(+) mass spectrum of the Suzuki reaction after 15 minutes.

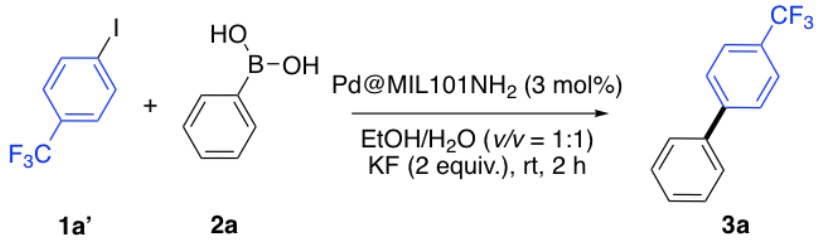

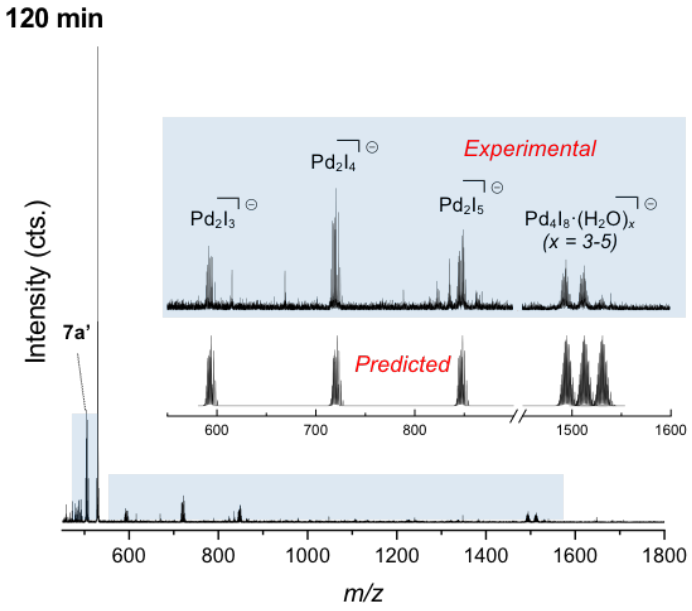

Figure S4. ESI(–)-MS of the Suzuki reaction with **1a'** after 120 min

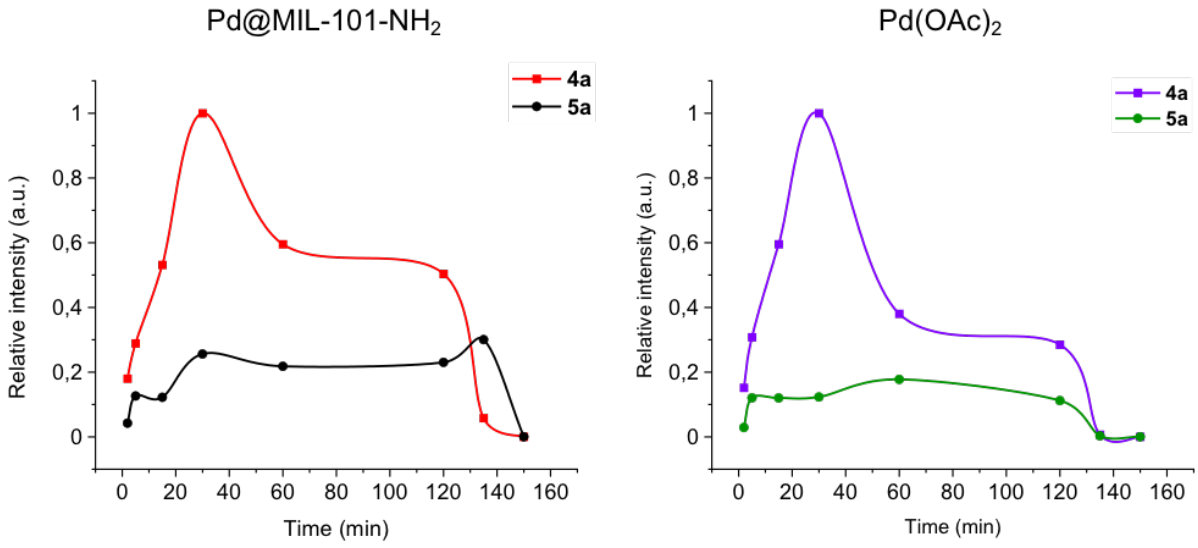

Figure S5. Relative abundance *vs.* time for tetramer **4a** and trimer **5a** using Pd@MOF (left) and $Pd(OAc)_2$ (right).

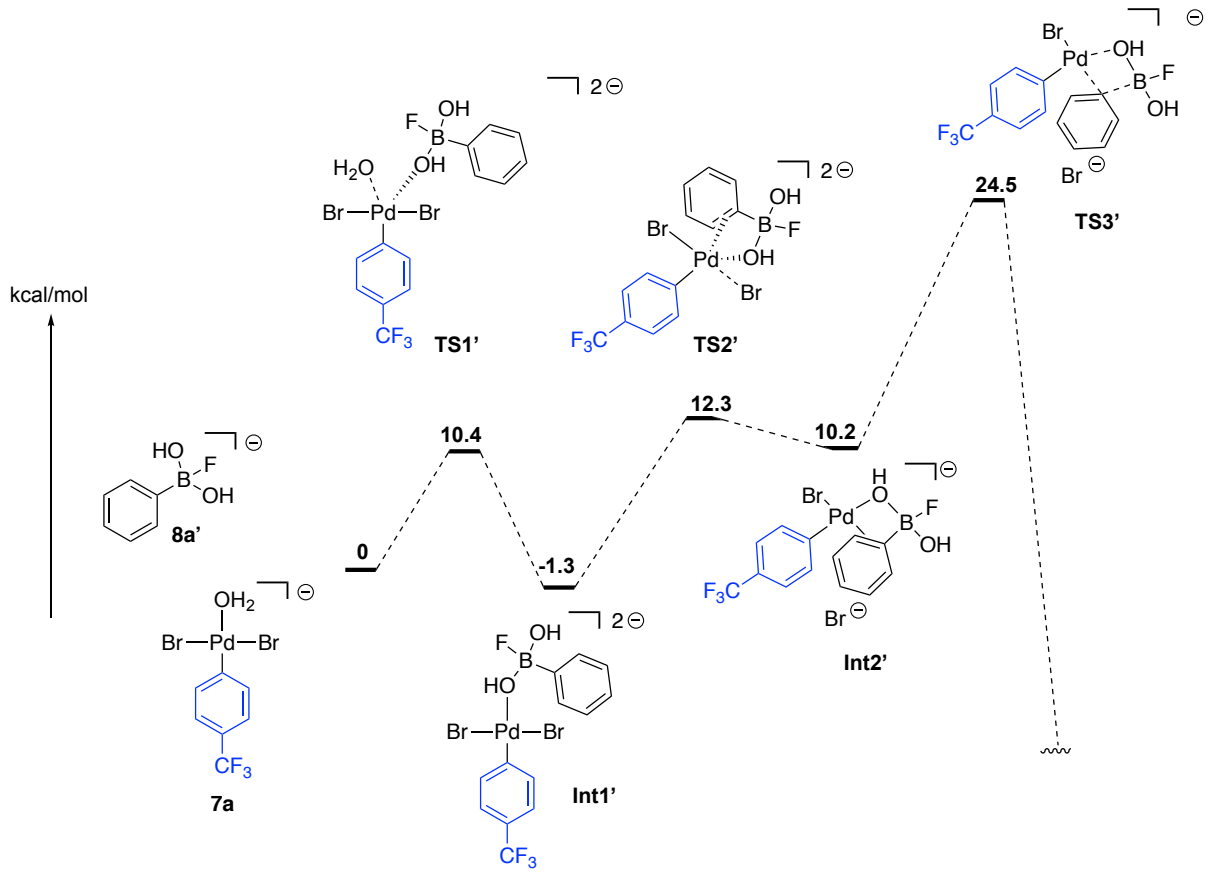

Figure S6. Free-energy profile for the transmetallation and reductive elimination steps from monomer **7a**

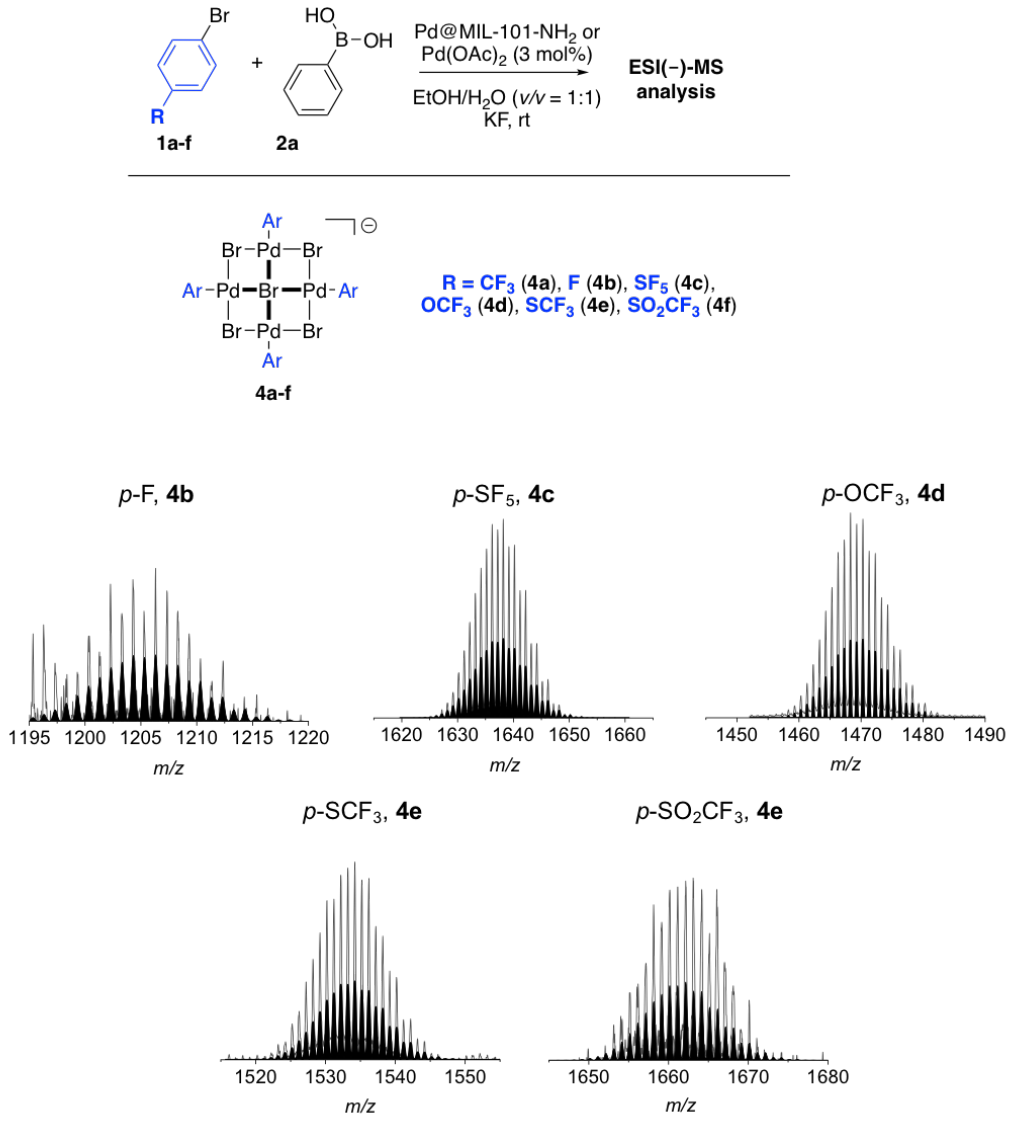

Figure S7. Detection of tetramers **4b**-**4f**. In grey experimental patterns, simulated in black.

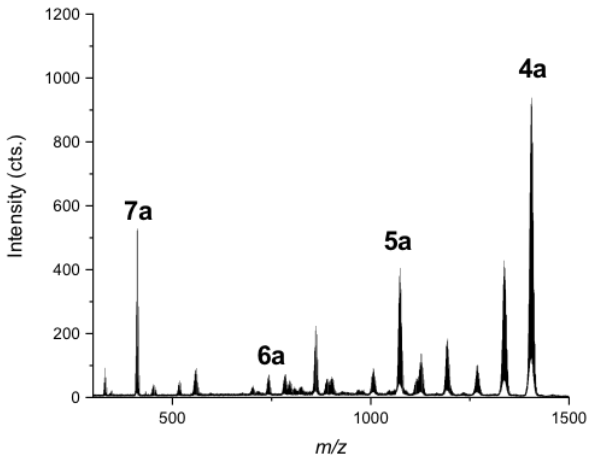

Figure S8. ESI(–)-MS spectrum of the Suzuki reaction using $Pd(OAc)_2$.

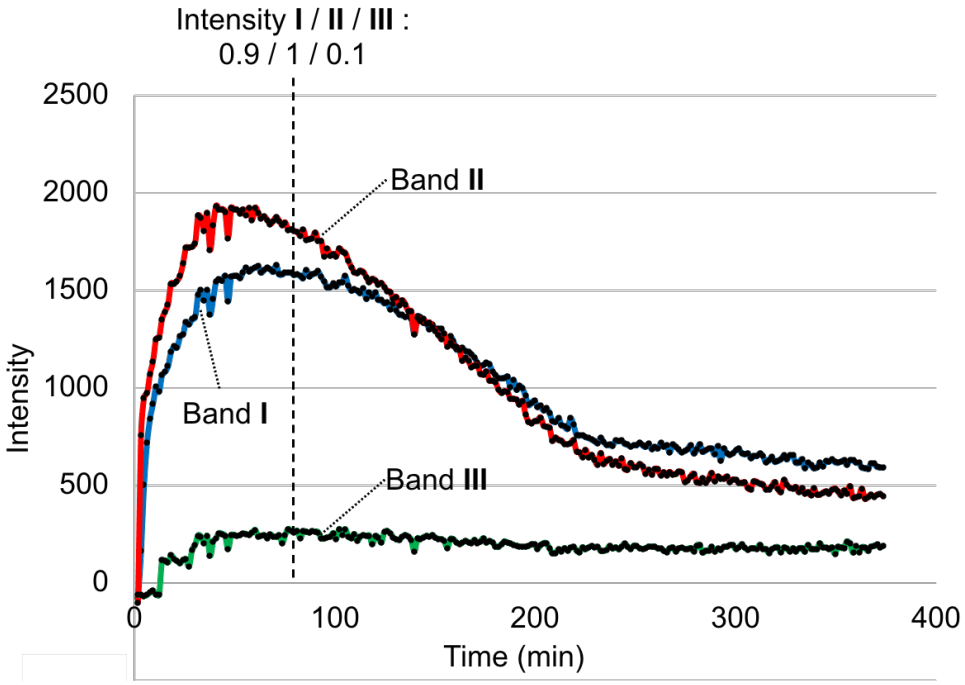

Figure S9. Intensity vs. time for bands **I**, **II** and **III**

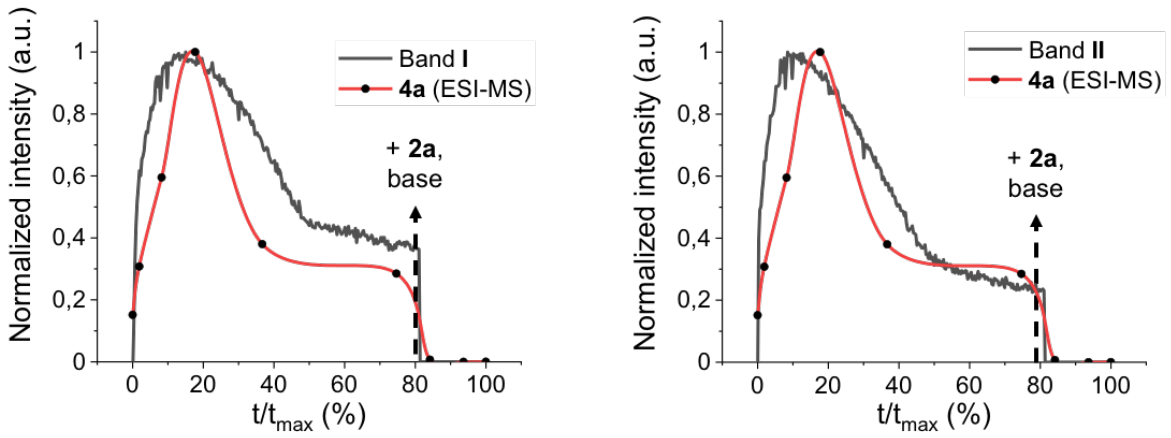

Figure S10. Correlation of the relative abundance of 4a with bands I (left) and II (right).

3. References

(1) Bochevarov, A. D.; Harder, E.; Hughes, T. F.; Greenwood, J. R.; Braden, D. A.; Philipp, D. M.; Rinaldo, D.; Halls, M. D.; Zhang, J.; Friesner, R. A. *Int. J. Quantum Chem.* **2013**, *113*, 2110–2142.

(2) Grimme, S.; Antony, J.; Ehrlich, S.; Krieg, H. *J. Chem. Phys.* **2010**, *132*.

(3) Becke, A. D. *J. Chem. Phys.* **1993**, *98*, 5648–5652.

(4) Lee, C.; Yang, W.; Parr, R. G. *Phys. Rev. B* **1988**, *37*, 785–789.

(5) Hay, P. J.; Wadt, W. R. *J. Chem. Phys.* **1985**, *82*, 299–310.

(6) Marten, B.; Kim, K.; Cortis, C.; Friesner, R. A.; Murphy, R. B.; Ringnalda, M. N.; Sitkoff, D.; Honig, B. *J. Phys. Chem.* **1996**, *100*, 11775–11788.

(7) Marenich, A. V.; Olson, R. M.; Kelly, C. P.; Cramer, C. J.; Truhlar, D. G. *J. Chem. Theory Comput.* **2007**, *3*, 2011–2033.